Chemical Engineering Journal 522 (2025) 167825

Contents lists available at ScienceDirect

Chemical Engineering Journal

journal homepage: www.elsevier.com/locate/cej

Turning waste into value: Fabrication of gas diffusion electrodes from biomass-derived materials for CO_2 electroreduction to formate☆

Guillermo Díaz-Sainz [a,*,1], Jose Antonio Abarca [a,1], Iker Uriarte-Porres [a], Álvaro Ramírez [b], Martín Muñoz-Morales [b], Ángel Irabien [a], Javier Llanos [b], Manuel Álvarez-Guerra [a]

[a] Departamento de Ingenierías Química y Biomolecular, Universidad de Cantabria, Avenida de los Castros s/n, 39005 Santander, Spain
[b] Departamento de Ingeniería Química, Facultad de Ciencias y Tecnologías Químicas, Ciudad Real, Universidad de Castilla-La Mancha, Ciudad Real 13071, Spain

ARTICLE INFO

Keywords:
Biomass-waste derivates
CO_2 Electroreduction
Formate
Gas diffusion electrodes
Typha dominguensis
Phragmites australis
Claudium mariscus

ABSTRACT

Climate change, driven predominantly by anthropogenic activities such as fossil fuel combustion, has led to significant greenhouse gas emissions. In response, the United Nations' COP28 has set an ambitious goal to reduce emissions by 43 % by 2030, with the aim of limiting global temperature rise to 1.5 °C. Among the various CO_2 mitigation strategies, Carbon Capture and Utilization (CCU) is particularly promising, especially the electrochemical reduction of CO_2 into valuable chemicals. This process not only curtails CO_2 emissions but also facilitates the production of renewable chemicals such as formic acid and formate. Gas diffusion electrodes (GDEs) are central to CO_2 electroreduction, with the microporous layer playing a critical role in preventing flooding and optimizing catalyst interaction. However, traditional carbon black-based microporous layers, such as those made from Vulcan XC-72R, raise environmental and health concerns. This study explores the use of biomass-derived materials, specifically lignocellulosic species, processed via hydrothermal carbonization, pyrolysis, and chemical activation. The results show that GDEs incorporating a biomass and Vulcan XC-72R (50 % wt) mixture achieve high formate concentrations (1.8 $g{\cdot}L^{-1}$) and Faradaic efficiency toward formate (80 %) at 90 $mA{\cdot}cm^{-2}$—performances that are comparable to or even superior to those of GDEs made solely with commercial Vulcan XC-72R. This demonstrates that these sustainable biomass-derived materials have great potential to effectively replace up to 50 % of carbon black materials and thereby reducing reliance on non-renewable resources, for the production of high-value chemicals from CO_2.

1. Introduction

Climate change, primarily driven by the combustion of fossil fuels such as coal, oil and gas, remains a critical global issue due to the emission of greenhouse gases like CO_2 and CH_4. These gases contribute to global warming, and the concentration of CO_2 has surpassed the critical threshold of 420 ppm [1]. Immediate action to reduce CO_2 emissions is essential to mitigate the impacts of climate change.

At the 29th United Nations Climate Change Conference (COP 29) held in Azerbaijan [2], it was reported that providing financial support to developing countries for the implementation of renewable energy and energy storage technologies is crucial for reducing reliance on fossil fuels. This support could also stimulate job creation and drive global economic growth. If these measures are implemented promptly, they could reduce global greenhouse gas emissions by 63 % by 2050 [3].

While low-carbon technologies show considerable promise in sectors like transport and construction [4], industries such as cement and steel face challenges due to the intrinsic CO_2 emissions associated with their production processes [5]. To address these challenges, decarbonization strategies focus on improving energy efficiency, adopting renewable energy sources, and deploying CO_2 capture, utilization, and storage (CCUS) technologies. CCUS technologies have gained significant attention for their potential to mitigate CO_2 emissions while producing value-added products through various technologies [6,7], including thermochemistry [8], photo-catalytic electroreduction [9] and electrochemical reduction [10].

Among these strategies, CO_2 electroreduction stands out as a particularly promising method for decarbonization. This approach

☆ This article is part of a Special issue entitled: 'CCUS' published in Chemical Engineering Journal.

* Corresponding author.
E-mail address: diazsg@unican.es (G. Díaz-Sainz).

[1] G. Díaz-Sainz and J.A. Abarca contributed equally to this work as first authors.

https://doi.org/10.1016/j.cej.2025.167825
Received 21 June 2025; Received in revised form 8 August 2025; Accepted 27 August 2025
Available online 28 August 2025

aligns with the increasing trend of electrification within the chemical industry [11] by storing excess renewable energy in chemical bonds and producing valuable products such as formic acid/formate [12], carbon monoxide [6], methane [13], methanol, and other C_2 products [14]. Formate, in particular, is a high-potential product for industrial-scale CO_2 electroreduction due to its efficiency in hydrogen storage, which is critical for the transition to a circular economy. Furthermore, formic acid is a valuable commodity in the CO_2 conversion market, with prices ranging from $500 to $1500 per ton [15], and it can also serve as fuel in fuel cells to generate electricity [16,17].

CO_2 electrochemical reduction can be achieved under ambient temperature and pressure, with product optimization through modification to metal-based catalysts, electrode potential adjustments, and pH control [18]. A variety of studies have investigated CO_2 electrochemical conversion to formate using different electrode configurations [19,20]. Among these, the most commonly effective configuration is the Gas Diffusion Electrode (GDE), which typically consists of three layers: a support layer, a microporous layer (MPL), and a catalytic layer (CL) [21]. In this configuration, CO_2 diffuses through the gas diffusion layer (GDL) to the catalytic layer, which can be in contact with either a liquid electrolyte [22,23] or a solid electrolyte (membrane) [24,25]. This structure enhances CO_2 electroreduction performance by increasing the active surface area and minimizing mass transfer resistances [26–29].

A major challenge in the fabrication of GDEs is ensuring reproducibility [30]. Variations in key properties, such as wettability, porosity, morphology and chemical stability, can significantly affect electrode performance [26,31,32]. Contamination by carbonate salts, which form when CO_2 reacts with hydroxide in the presence of cationic species like potassium and sodium, is a common issue [33,34].

Most research has focused on optimizing the catalytic layer by using various electrocatalysts, especially metal-based catalysts, due to their high efficiency in CO_2 conversion [35–42].

However, limited attention has been given to the materials used for the MPL. Traditional commercial MPLs typically consist of a carbonaceous material, such as carbon black, to reduce ohmic losses and enhance electron transfer, combined with a polymer, such as polytetrafluoroethylene (PTFE), to modulate wettability [43]. The most commonly used commercial carbon black is Vulcan XC-72R, valued for its optimal balance of specific surface area and electrical conductivity [44,45]. While alternative materials such as carbon nanofibers (CNFs) and carbon nanotubes (CNTs) have been explored to improve performance, their production process, often involving the high-temperature incomplete combustion of petroleum hydrocarbons, generate harmful compounds, including volatile organic compounds (VOCs), nitrogen oxides (NOx), sulfur oxides (SOx), methane (CH_4), and carbon dioxide (CO_2), making it difficult to improve their environmental footprint and sustainability [46,47]. Furthermore, the production of carbon black is heavily reliant on fossil fuels, further increasing dependence on non-renewable resources and contributing to environmental degradation [48].

To mitigate these environmental concerns, it is essential to explore more sustainable alternatives with lower environmental impacts. One promising approach involves the use of waste lignocellulosic materials [49–51], which serve as a valuable raw residue for producing carbonaceous materials with physicochemical characteristics close to carbon black after some thermochemical treatments. Consequently, carbon powders derived from lignocellulosic biomass are emerging as sustainable alternatives to conventional fossil fuel-based carbon blacks. What's more, some lignocellulosic biomasses can become toxic wastes if previously used in phytoremediation processes targeting organic and metallic pollutants [52–56], or as biosorbents [57,58], and therefore require proper management. Previous studies on biomass-wastes have confirmed their viability as catalysts for H_2O_2 electrogeneration and pollutant electrooxidation in water decontamination [59]. However, the selection of biomass residues in the present study, Typha dominguensis (TD), *Phragmites australis* (PA), and Claudium mariscus (CM), was based not only on their viability for environmental remediation but also on the need to address specific ecological and management challenges in local natural wetlands.

In particular, the overaccumulation of senescent biomass from these species in protected areas, such as "Las Tablas de Daimiel" National Park (39°08'42"N 3°42'07"W), exacerbated by prolonged droughts, has intensified the risk of wildfires and eutrophication, highlighting the urgent need for biomass management [60]. In the case of TD, its cultivation also supports biodiversity conservation, as this species is experiencing population decline due to hydric stress from recurring droughts and interspecies competition, raising concerns over its local conservation. Valorizing these biomasses contributes to closing the circular economy loop by enabling pollutant removal and providing carbonaceous material for incorporation into the MPL used in the electrochemical reduction of CO_2.

Thus, the primary objective of this study is to evaluate the feasibility of fabricating GDEs for continuous CO_2 electroreduction to formate utilizing three distinct biomass sources (TD, PA and CM), as sustainable alternatives to conventional commercial materials, such as Vulcan XC-72R. This novel approach aligns with circular economy principles by promoting the reuse and valorization of biomass waste.

2. Methodology

2.1. Synthesis of carbon materials from lignocellulosic wastes

Three biomass species evaluated were *Typha domingensis* (TD) (cellulose 11.5 ± 0.1 %, hemicellulose 40 ± 0.1 %, lignin 45 ± 0.1 %), *Phragmites australis* (PA) (cellulose 9.5 ± 0.1 %, hemicellulose 48 ± 0.1 %, lignin 33 ± 0.1 %) and *Cladium mariscus* (CM) (cellulose 13 ± 0.1 %, hemicellulose 41 ± 0.1 %, lignin 40 % ± 0.1), all collected from 'Tablas de Daimiel' (39°08'42"N 3°42'07"W), a natural wetland located in the province of Ciudad Real, Spain. Three plant species commonly used in phytoremediation and constructed wetland systems for the remediation of water and soil are known for their ability to retain a broad range of pollutants, including both organic compounds and heavy metals. After serving in these treatment applications, appropriate post-treatment handling of the biomass is required [54].

After an initial cleaning with Milli-Q water, the samples underwent hydrothermal carbonization (HTC) at 200 °C for 2 h under self-generated pressure in a stainless-steel Parr autoclave (biomass to water ratio of 130 $g{\cdot}L^{-1}$). After the initial soft treatment, the resulting hydrochars followed two different processing pathways. One pathway involved pyrolysis at 1000 °C under a N_2 atmosphere (150 mL min^{-1}), while the other consisted of chemical activation using KOH at 600 °C, also under the same inert atmosphere. For the chemical activation, the corresponding biomass-derived hydrochars were mixed with a 50 % w/v KOH solution at a 1:5 w/w hydrochar:KOH ratio. In both procedures, the heating rate was maintained at 2 $°C{\cdot}min^{-1}$, and the final temperature was held for 30 min, with intermediate dwell times of 30 min at 300, 500 and 750 °C. The result of relevant physicochemical properties of the synthesized carbon materials for electrochemical applications, such as the A_{D1}/A_G ratio obtained from Raman spectroscopy, electrical conductivity, and specific surface area, are summarized in Table S1. The methodologies employed for their determination are described in greater detail elsewhere [59].

2.2. Cathode fabrication

The GDE configuration employed in this study comprises three primary components: a carbonaceous support (TGP-H-60), a MPL, and a CL. Toray carbon paper (Teflonated Paper, TGP-H-60) serves as the carbonaceous support. The GDE features a geometric surface area of 10 cm^2.

The MPL was initially prepared using the air-brushing technique, a widely adopted method due to its simplicity, scalability, and ability to

produce uniform coatings, similar as previous studies to make a rigorous comparative assessment [23]. The ink formulation for air-brushing involves a 40:60 w/w carbon black (or alternative lignocellulosic biomass-derived materials such as TD, PA, or CM) to polytetrafluoroethylene (PTFE) dispersion (60 wt% in H_2O, Sigma-Aldrich). This mixture is diluted in isopropanol to achieve a 3 wt% suspension and sonicated for 30 min to ensure homogeneity.

The prepared ink is then applied to the carbon fiber support via air-brushing, building up the MPL to a carbon black loading of 2 mg·cm^{-2}. Post-deposition, the MPL undergoes sintering at 350 °C for 1800 s in a muffle furnace (J.P. Selecta, Select-Horn-TFT) to enhance material adhesion and structural integrity.

The CL is applied at the top of the MPL using the same air-brushing technique. The catalytic ink comprises bismuth oxide (Bi_2O_3, 99.99 % trace metal basis, 90–210 nm particle size, Sigma-Aldrich) dispersed in Nafion (Nafion D-521 dispersion, 5 % w/w in water and 1-propanol, ≥0.92 meq/g exchange capacity) at 70:30 w/w ratio. This mixture is diluted in isopropanol and sonicated under the same conditions as the MPL ink. The bismuth catalyst is loaded at 0.75 mg·cm^{-2}. The GDEs fabricated using carbon materials derived from the valorization of residual organic biomass are herein referred to as BioRem-GDEs. Both air pressure and ink flow rate were controlled and fixed at 0.5 bar and 20 mL·h^{-1}, respectively. The ink was deposited onto a heated surface maintained at approximately 70 °C. Deposition was carried out until the electrode reached the desired final loading, monitored by continuous weighing.

While air-brushing was initially employed for MPL synthesis, this study also explores vacuum deposition as an alternative technique, prompted by the unsatisfactory results obtained with air-brushing. Vacuum deposition allows for more precise control over layer uniformity and thickness—critical parameters for ensuring reproducibility and optimizing performance in electrochemical reactions [30]. The vacuum deposition setup consists of a vacuum pump (Millipore Milivac Maxi 5D1P014M04), a vacuum column with a Kitasato flask (Millipore XX1504705), a filtration funnel with a porous plate (Millipore XX1004704), circular filter paper (Filter-Lab), and metal tweezers (Millipore XX1004703). A schematic of the setup is provided in Fig. S1 of the Supplementary information.

2.3. Cathode characterization

To evaluate the structural and surface modifications induced during electrochemical tests, the electrodes were characterized both before and after operation using three analytical techniques. Surface images were obtained using HR-SEM technology with a ZEISS GeminiSEM 500 HR-SEM. *Image J* software was used to quantify the number and width of cracks observed in SEM micrographs of GDE surfaces prepared using the vacuum deposition technique. Surface elemental analysis was conducted through Energy Dispersive X-ray Spectroscopy (EDS), integrated with the SEM system and to evaluate the hydrophobicity/hydrophilicity of the electrode surfaces, the static contact angle (sCA) was measured through the static sessile drop method using an Attention Theta Optical Tensiometer (Biolin Scientific), controlled via One attention software and a high-definition camera.

The physicochemical characterization of the carbonaceous materials synthesized from lignocellulosic waste was detailed elsewhere [59].

2.4. Experimental setup

The electrochemical performance of the fabricated BioRem-GDEs was evaluated using a continuous-flow, two-compartment filter-press electrochemical reactor (Micro Flow Cell, ElectroCell A/S) operating under standard conditions. The experimental setup included peristaltic pumps (Watson Marlow 320), electrolyte reservoirs, and a potentiostat–galvanostat (Arbin Instruments, MSTAT4) for precise control and monitoring of electrochemical parameters, as shown in Fig. 1.

Within the reactor (Fig. 2), the BioRem-GDEs were placed in the cathodic compartment, where the electrochemical reduction of CO_2 to formate was carried out under conditions similar to those used in previous studies [23]. This compartment featured two inlets:

(1) Gaseous CO_2 supply: pure CO_2 was introduced at a flow rate of 200 mL·min^{-1} and diffused through the carbonaceous fiber paper to reach the catalytic layer.
(2) Catholyte circulation: an aqueous solution composed of 0.5 M KCl and 0.45 M $KHCO_3$ (both from PanReac AppliChem) (pH ~ 8) was circulated at a flow rate of 0.57 mL·min^{-1}·cm^{-2}. The slightly basic pH of the catholyte helps suppress the hydrogen evolution reaction (HER) at the cathode surface, thereby improving the selectivity toward formate production. However, it is important to note that under these alkaline conditions, a portion of the CO_2 may be lost due to the formation of carbonate and bicarbonate species.

The anodic compartment was supplied with 1 M KOH (pH ~14) at the same specific flow rate per geometric surface area (0.57

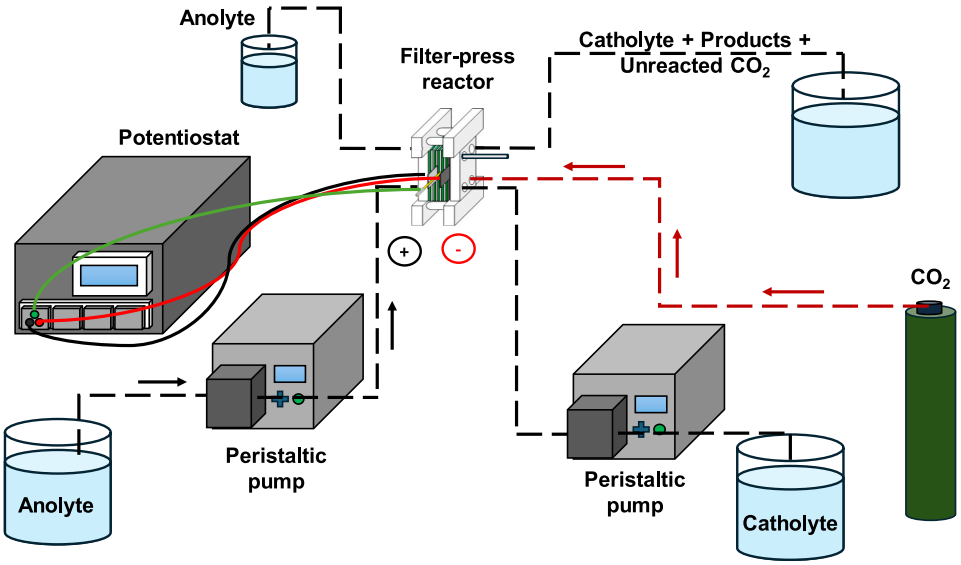

Fig. 1. Experimental set up used for the tests of BioRem-GDEs for the continuous CO_2 electrocatalytic reduction to give formate.

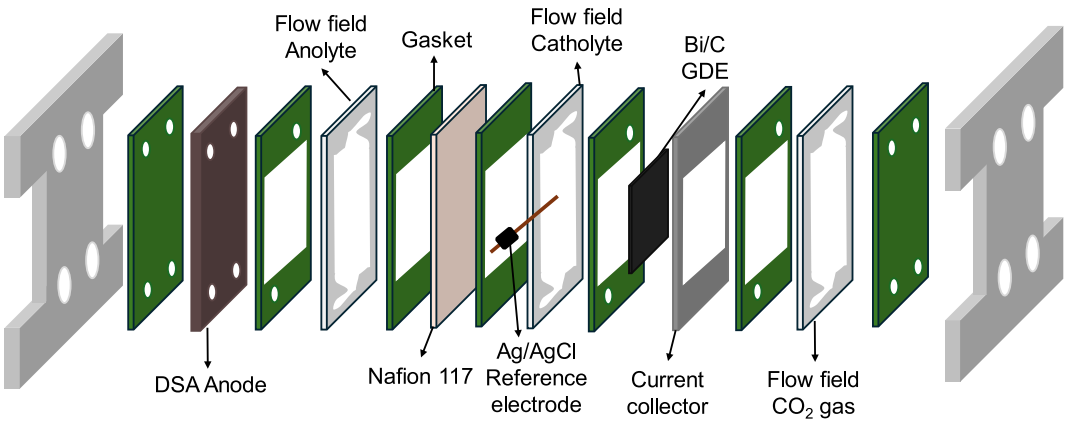

Fig. 2. Filter press cell configuration used for the continuous CO_2 electrocatalytic reduction to give formate using BioRem-GDEs. Adapted from [61].

$mL \cdot min^{-1} \cdot cm^{-2}$). A dimensionally stable anode (DSA/O_2), consisting of Ir-MMO (mixed metal oxide) on platinum, was used as the counter electrode to facilitate the oxygen evolution reaction (OER).

A leak-free Ag/AgCl reference electrode (3.4 M KCl) was placed near the working electrode in the cathode compartment to ensure accurate measurement of the working electrode potential. The two compartments were separated by a Nafion 117 cation exchange membrane (thickness: 0.180 mm; exchange capacity: >0.9 meq/g; Alfa Aesar) which prevented product crossover while maintaining ionic conductivity.

Experiments were performed in continuous single-pass mode, with both catholyte and anolyte flowing through the reactor without recirculation. Each test was conducted in duplicate under ambient conditions (101,325 Pa and 20 °C) for a minimum duration of 3600 s.

The main objective was to evaluate the performance of BioRem-GDEs fabricated from waste-derived materials, in comparison to conventional carbon-based electrodes, under a current density of 90 $mA \cdot cm^{-2}$ [23]. Samples were collected every 20 min over a total duration of 1 h.

Formate concentration was quantified using ion chromatograph (Dionex ICS 1100 equipped with an AS11−HC column), using Na_2CO_3 (4.5 mM) as the eluent at a flow-rate of 1 $mL \cdot min^{-1}$.

Based on the measured formate concentrations, the electrochemical performance was evaluated through key of merit: Faradaic Efficiency (FE), production rate, and energy consumption [19]. The equations for calculating each of these figures of merit are detailed in the Supplementary information.

3. Results

3.1. Assessment of deposition techniques for MPL fabrication

The first BioRem-GDEs for CO_2 electroreduction to formate were fabricated using the air-brushing technique to prepare the MPL in order to compare previously developed GDEs under identical experimental setups and comparable operating conditions [23,40,62]. The initial BioRem-GDEs were evaluated at a current density of 90 $mA \cdot cm^{-2}$, with both catholyte and anolyte flowing at 0.57 $mL \cdot min^{-1} \cdot cm^{-2}$ based on geometric area in their respective compartments.

However, the air-brushing technique exhibited low reproducibility in the fabrication of the MPL, as shown in Table S2 for MPLs prepared from TD 1000 °C, CM 1000 °C, TD 600 °C/KOH, PA 600 °C/KOH, and CM 600 °C/KOH. Moreover, in the case of MPLs derived from PA 1000 °C, no formate was detected in the output stream of the electrochemical reactor, indicating a complete lack of activity under the tested conditions.

Due to unsatisfactory initial results, the electrode fabrication method was revised by replacing air-brushing with vacuum deposition for MPL preparation, aiming to enhance BioRem-GDE performance through more uniform and controlled deposition of biomass-derived carbon.

Vacuum deposition was selected instead of air-brushing during MPL preparation in response to the operational challenges associated with air-brushing carbon black materials obtained from waste biomass, particularly the obstruction of the air-brushing system by larger particles. To evaluate the effectiveness of this alternative approach, preliminary tests were conducted using the same materials as in the reference electrodes, specifically Vulcan XC-72R as the carbon black.

All experimental tests were conducted under consistent operational conditions, maintaining a current density of 90 $mA \cdot cm^{-2}$ and a constant electrolyte flow rate of 0.57 $mL \cdot min^{-1} \cdot cm^{-2}$. A comparative analysis of the two deposition techniques, presented in Fig. 3, reveals that vacuum deposition resulted in slightly improved performance in terms of formate concentration, reaching 1.97 $g \cdot L^{-1}$ (Fig. 3a). This enhancement corresponds to a higher formate production rate of 4.17 $mmol \cdot s^{-1} \cdot m^{-2}$, compared to 3.62 $mmol \cdot s^{-1} \cdot m^{-2}$ achieved using the air-brushing method.

Moreover, a notable difference was observed in Faradaic Efficiency toward formate, with vacuum deposition exhibiting an approximately 15 % higher Faradaic Efficiency. This indicates a more efficient utilization of the supplied charge, with a greater proportion being directed toward formate production.

As illustrated in Fig. 3b, the vacuum deposition method exhibits lower energy consumption compared to the air-brushing technique. This improvement could be attributed to the more homogeneous, efficient, and controlled deposition of MPL material, positioning vacuum deposition as a more energy-efficient and potentially more sustainable method. To confirm this hypothesis, SEM and EDS images were taken of the electrodes prepared by both methods. Fig. 4 presents a comparative visualization of the two electrodes. As can be observed, the electrodes prepared by airbrushing exhibit a surface where the particles tend to agglomerate, which is clearly visible both in the SEM image (Fig. 4a and b) and in the surface atomic distribution provided by the EDS analysis (Fig. 4c and d). Although the elemental composition of the surface is similar (60.94 % C, 38.99 % F of air-brushing vs 68.5 % C, 31.4 % F of vacuum-deposited), the electrode prepared by air-brushing shows discrete superficial nodules, indicative of the heterogeneous distribution of the material. In contrast, the vacuum-deposited electrode displays a more uniformly distributed layer across the surface. Additionally, vacuum deposition facilitated the formation of well-defined cracks across the GDE surface, which play a crucial role in optimizing the electrolyte–electrode interface. These structural features help mitigate flooding within the GDE structure, thereby enhancing CO_2 transport to the catalyst's active sites [63,64].

Such advantages of the vacuum deposition techniques are particularly relevant for industrial applications, where optimizing both production efficiency and resource utilization are critical. Another key

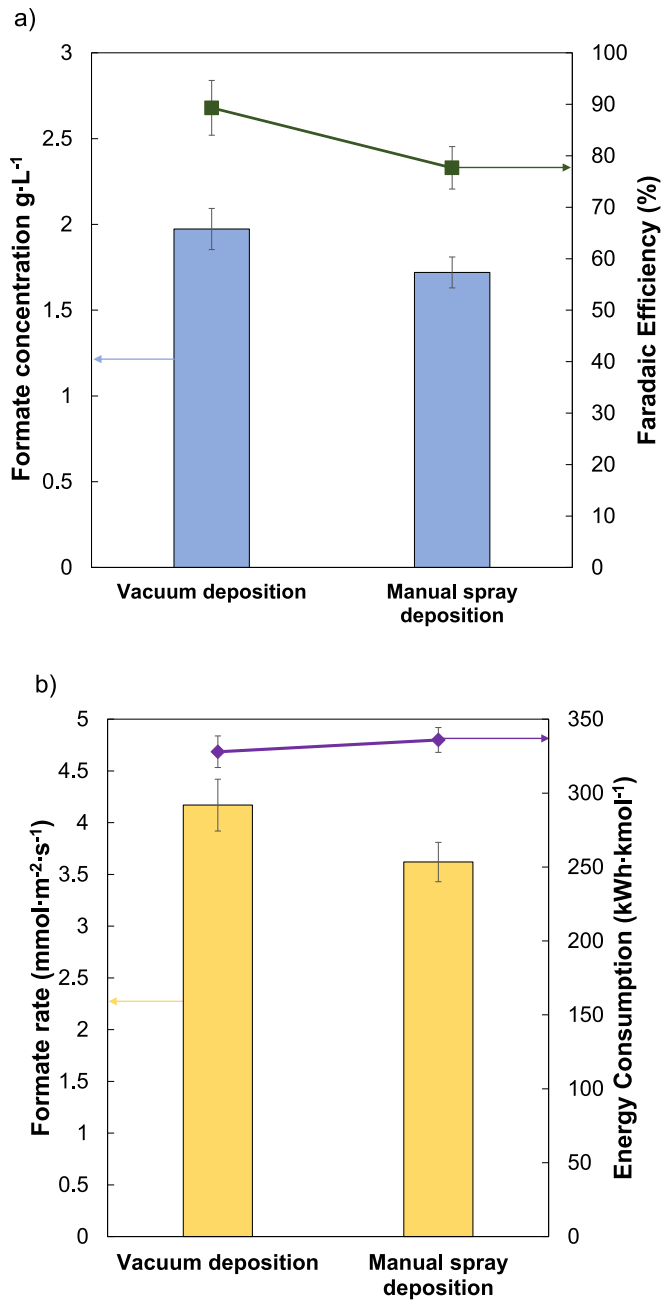

Fig. 3. Performance evaluation of Vulcan XC-72R as a MPL material using different deposition techniques under standardized process conditions (current density = 90 mA·cm^{-2}; catholyte and anolyte flow rates = 0.57 mL·min^{-1}·cm^{-2}, based on geometric surface area). (a) Formate concentration (g·L^{-1}) and Faradaic efficiency for formate (%); (b) formate production rate (mmol·s^{-1}·m^{-2}) and energy consumption (kWh·kmol^{-1}).

aspect to highlight is the reproducibility of the results. Across all experiments, a relative standard deviation (RSD) below 6 % was recorded, demonstrating high consistency and underscoring the robustness of the vacuum deposition method under comparable operating conditions.

The favorable outcomes of this comparative study confirm the reproducibility and reliable performance of vacuum deposition, validating it as a suitable and scalable technique for GDE fabrication. Accordingly, all subsequent experiments were conducted using BioRem-GDEs prepared via vacuum deposition.

3.2. Performance of BioRem-GDEs fabricated via vacuum deposition

Following the assessment of the technical feasibility of preparing MPLs via vacuum deposition using Vulcan XC-72R materials, the next step is to evaluate the feasibility of employing BioRem-GDEs with MPLs fabricated using this technique. However, due to the low electroreduction efficiency and poor reproducibility observed in electrodes made from biomass waste derivates chemically activated with KOH at 600 °C, efforts focused on materials pyrolyzed at 1000 °C. By analyzing the values of the properties presented in Table S1, it was observed that the materials pyrolyzed at 1000 °C exhibited significantly higher electrical conductivity (ranging from 76 to 211 S·m^{-1}) and A_{D1}/A_G ratios (ranging from 1.81 to 2.00). The higher conductivity can reduce ohmic losses, while the greater degree of structural disorder, reflected in higher A_{D1}/A_G ratios and associated with defects such as vacancies, edges, and heteroatoms, may serve as nucleation sites for CO_2 adsorption and facilitate the formation of CO_2^- intermediates, while are critical for formate production [65]. These values outperform those obtained with the materials chemically activated with KOH, which showed lower conductivity values (between 12 and 39 S·m^{-1}) and A_{D1}/A_G ratios (between 1.48 and 1.74). This highlights the strong influence of these physicochemical parameters on CO_2 electroreduction performance. Nevertheless, a substantial increase in specific surface area did not correlate with improved electrochemical performance, as the KOH-activated materials, despite having much higher surface areas (between 1060 and 1603 m^2·g^{-1}) compared to the pyrolyzed materials (between 146 and 308 m^2·g^{-1}), consistently showed inferior results.

Table 1 summarizes the key results obtained with the BioRem-GDEs, whose MPLs were fabricated via vacuum deposition.

Initially, MPLs based on biomass-derived hydrochars treated at 1000 °C showed varying performance in CO_2 electroreduction. TD-derived cathodes reached a maximum formate concentration of 1.48 g·L^{-1}, comparable to Vulcan XC-72R, but exhibited low reproducibility and moderate Faradaic Efficiency (66.9 %). Additionally, energy consumption was notably high (~2000 kWh·kmol^{-1} at 90 mA·cm^{-2}), reflecting poor electrochemical efficiency. PA-based MPLs slightly outperformed TD in formate production (1.55 g·L^{-1}) and Faradaic Efficiency (~70 %), while significantly reducing energy demand to 477 kWh·kmol^{-1}, suggesting better charge utilization and catalytic behavior. In contrast, CM yielded the lowest formate concentration (0.78 g·L^{-1}) and Faradaic Efficiency (35.5 %), with poor reproducibility (RSD 66 %) and high energy consumption (664 kWh·kmol^{-1}), indicating limited suitability for CO_2 electroreduction. It can also be observed that the materials treated at 1000 °C exhibited differences in structural order and, more notably, in electrical conductivity. Among the three materials, CM exhibited the lowest A_{D1}/A_G ratio at 1.81, while TD and PA showed higher values of 1.99 and 2.00, respectively. As previously discussed, a higher ratio appears to be beneficial for CO_2 electroreduction activity, as is also observed in O_2 electroreduction for H_2O_2 production [66]. However, the most significant difference lies in electrical conductivity. TD and PA demonstrated conductivities of 178 and 211 S·m^{-1}, respectively, values comparable to that of commercial carbon black Vulcan XC72R (277 S·m^{-1}) [67]. In contrast, CM exhibited a much lower conductivity of 76 S·m^{-1}, which is considerably below that of the other carbons and represents one of the main factors contributing to its inferior performance. Overall, PA exhibited the most promising balance between efficiency, energy consumption, and performance consistency among the tested lignocellulosic biomass-derived materials.

The significantly higher RSD values observed for biomass-based electrodes compared to pure Vulcan electrodes can be attributed to the inherent variability and heterogeneity of biomass-derived carbons. These materials typically exhibit broad distributions in particle size, surface area, and chemical functionalities, which adversely affect the uniformity and reproducibility of electrode fabrication. In contrast, Vulcan XC-72R is a well-characterized commercial carbon with consistent and uniform properties, leading to more reproducible electrode

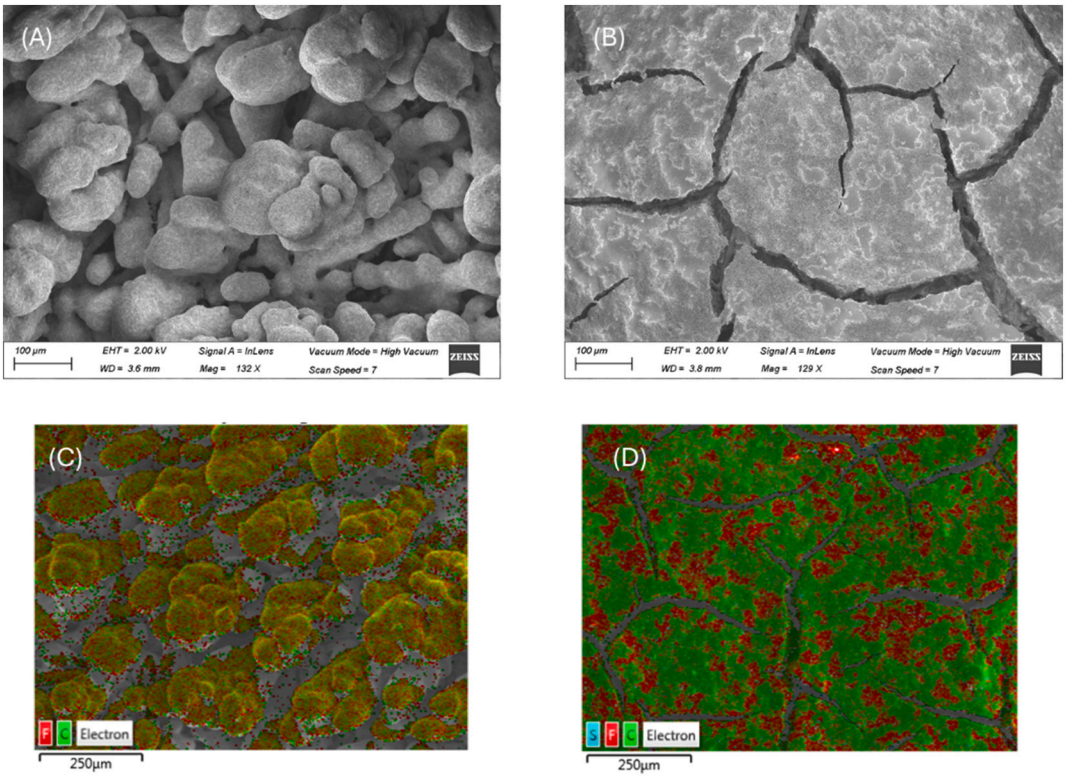

Fig. 4. Comparison of SEM and EDS images of electrode surface using different deposition techniques: (a) SEM air-brushing; (b) SEM vacuum deposition, (c) EDS air-brushing, (d) EDS vacuum deposition. All electrodes were synthesized with 100 % Vulcan XC-72R.

Table 1
Performance of BioRem-GDEs incorporation MPLs prepared from TD 1000 °C, PA 1000 °C and CM 1000 °C, fabricated via vacuum deposition.

MPL material	Cathode voltage (V)	Absolute cell voltage (V)	[$HCOO^-$] ($g{\cdot}L^{-1}$)	Production rate ($mmol{\cdot}s^{-1}{\cdot}m^{-2}$)	FE (%)	EC ($kWh{\cdot}kmol^{-1}$)	RSD (%)
TD 1000 °C	−2.34	4.06	1.48	3.117	66.84	325	96.38
PA 1000 °C	−2.41	6.24	1.55	3.269	70.09	477	54.06
CM 1000 °C	−2.58	4.40	0.78	1.655	35.49	664	66.19
Vulcan XC-72R	−2.20	5.45	1.97	4.166	89.27	328	5.97

preparation.

Based on these results, issues related to both performance and reproducibility were identified. To enhance the homogeneity and performance of the electrodes, and to reduce the variability observed in previous results, the MPL composition was modified by replacing 50 % of the commercial Vulcan XC-72R with lignocellulosic biomass-derived materials.

3.3. Improving electrode performance and homogeneity through biomass waste-derived materials

Fig. 5 includes the results regarding formate concentration, Faradaic efficiency for formate, production rate, and energy consumption for the BioRem-GDEs, whose MPL consists of a 50:50 blend of commercial Vulcan XC-72R and previously defined carbonaceous materials. The specific material combinations evaluated include: (i) 50 % TD 1000 °C – 50 % Vulcan XC-72R, (ii) 50 % PA 1000 °C – 50 % Vulcan XC-72R, and (iii) 50 % CM 1000 °C – 50 % Vulcan XC-72R.

As illustrated in Fig. 5a, the BioRem-GDE fabricated using a 50 % TD 1000 °C and 50 % Vulcan XC-72R mixture exhibits a lower formate concentration of 1.44 $g{\cdot}L^{-1}$, compared to the 1.97 $g{\cdot}L^{-1}$ achieved with electrodes prepared exclusively from commercial carbon black. Correspondingly, the CO_2 electroreduction system employing this TD-based composite yields the lowest formate production rate among all materials evaluated. In contrast, the GDE combining PA 1000 °C and Vulcan XC-72R in equal proportions exhibits a production rate (3.71 $mmol{\cdot}s^{-1}{\cdot}m^{-2}$) and formate concentration (1.8 $g{\cdot}L^{-1}$) comparable to those achieved with pure Vulcan XC-72R, indicating that this blend maintains electrochemical performance while partially substituting the commercial carbon material. Although the addition of TD 1000 °C allows for a moderately adequate production rate, the PA 1000 °C blend appears to deliver a more balanced and robust performance.

Fig. 5a also shows the Faradaic efficiency associated with formate production during the electroreduction process. All materials evaluated exhibit relatively high Faradaic Efficiency values, exceeding 65 %. Notably, the PA-1000 °C + Vulcan XC-72R blend achieves a Faradaic Efficiency of nearly 80 %, indicating superior selectivity toward formate and positioning it as the most promising material combination in terms of both efficiency and product selectivity. The CM 1000 °C + Vulcan XC-72R mixture also demonstrates good selectivity, although its performance does not significantly exceed or match that of the PA-based electrodes.

In terms of energy consumption (Fig. 5b), all tested BioRem-GDEs containing 50 % Vulcan XC-72R display reduced energy requirements relative to the benchmark value of 328 $kWh{\cdot}kmol^{-1}$ for the pure Vulcan-based GDE. Specifically, energy consumption for the blended materials consistently remained above 250 $kWh{\cdot}kmol^{-1}$, indicating a meaningful improvement in energy efficiency.

Collectively, these results suggest that the PA-1000 °C + Vulcan XC-72R (50:50) composition strikes the optimal balance across key

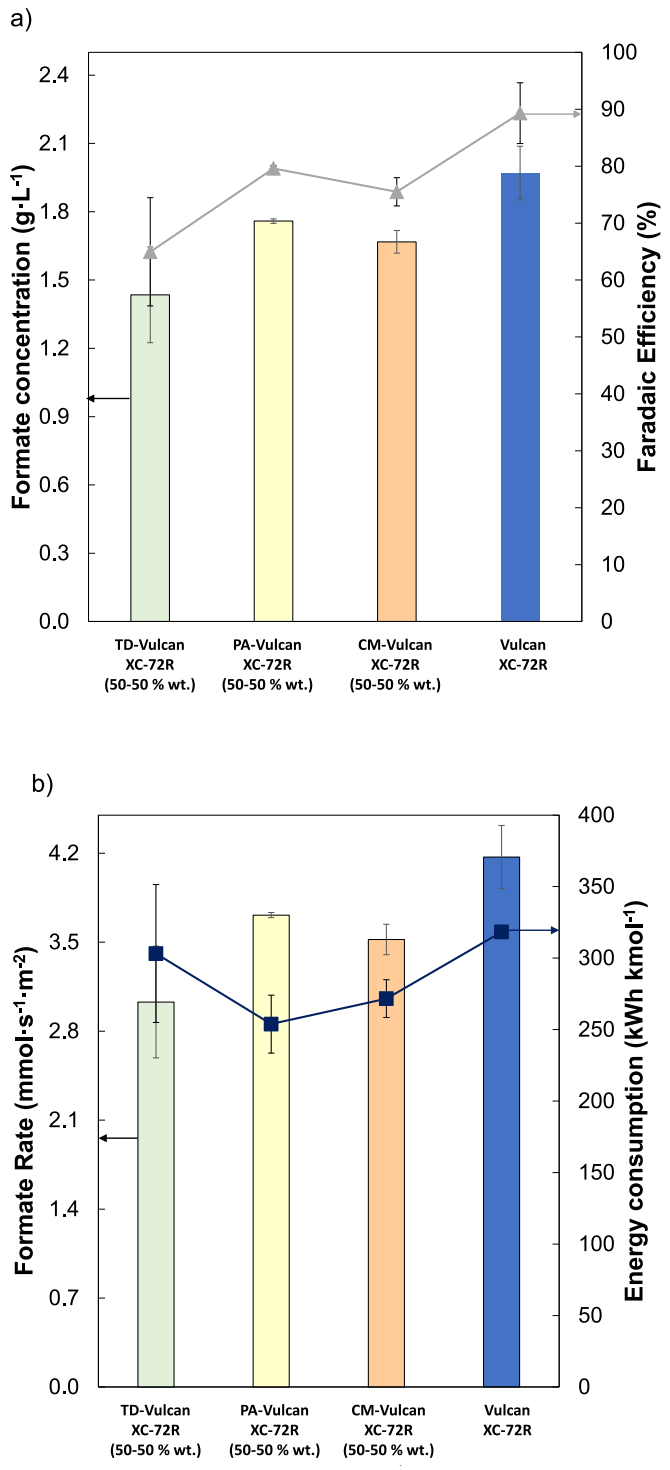

Fig. 5. Performance evaluation of BioRem-GDEs incorporating 50 wt% Vulcan XC-72R in the MPL, fabricated via vacuum deposition. Tests were conducted at a current density of 90 mA/cm^2, with catholyte and anolyte flow rates per geometric surface area of 0.57 mL·min^{-1}·cm^{-2}. Evaluated metrics include: (a) formate concentration (g·L^{-1}) and Faradaic efficiency for formate (%) and (b) formate production rate (mmol·s^{-1}·m^{-2}) and energy consumption of the process (kWh·kmol^{-1}).

performance metrics—achieving high formate productivity, outstanding Faradaic efficiency, and reduced energy consumption—positioning it as the most promising alternative to fully commercial materials for sustainable CO_2 electroreduction. Notably, the reproducibility of these electrode fabrications is exceptional, with most materials exhibiting a significantly lower RSD than the GDE made with commercial Vulcan XC-72R. The only exception is the TD 1000 °C + Vulcan XC-72R (50:50), which has an RSD of approximately 15 %. These findings underscore the technical feasibility of utilizing these alternative materials for CO_2 electrochemical reduction to formate, while minimizing the reliance on commercial Vulcan XC-72R.

3.4. Discussion of the results based on the characterization of the electrodes BioRem-GDEs

Synthesized PA and Vulcan XC-72R electrodes were analyzed using SEM before and after the electroreduction experiments. This approach allows for a direct comparison of the morphological changes induced by the process, as well as an assessment of the influence of the GDL carbonaceous material on the structural stability of the electrode. In parallel, EDS was employed to determine the elemental composition of the surface and to identify the key elements remaining after the electroreduction process. Representative SEM images are displayed in Fig. 6, whereas the corresponding EDS elemental mapping is provided in Fig. 7.

Fig. 6a shows that the electrode prepared exclusively with Vulcan XC-72R displays a flat, uniform and homogeneous surface morphology. In contrast, the incorporation of the carbonaceous material obtained from PA in a 1:1 ratio with Vulcan XC-72R (Fig. 6e) results in a more heterogeneous structure, with noticeable loss of the uniformity observed in the previous case. This heterogeneity is particularly evident in the electrode fabricated with PA 1000 °C MPL, as shown in Fig. 6c. Moreover, both the number and size of cracks on the MPL surface were found to influence the electrocatalytic performance of the cathodes. These parameters were manually quantified using the ImageJ software, and a correlation between crack size and Faradaic Efficiency was confirmed. For the PA-1000 °C sample (17 cracks mm^{-2}), the average crack size was approximately 18 μm, for the Vulcan XC-72R electrode (43 cracks mm^{-2}), the cracks measured around 158 μm. In the 50–50 % mixture (76 cracks mm^{-2}), crack size averaged 63 μm. A clear trend was observed, the larger the crack size, the higher the Faradaic Efficiency. This correlation is illustrated in Fig. S2. In all cases, the electrode surfaces exhibit evident signs of degradation after finishing the electroreduction experiments. The distinct structural features present in the unused samples are markedly reduced or lost after the electrochemical process, indicating substantial alterations in surface morphology.

Furthermore, EDS analysis (Fig. 7) highlights significant changes in the Fluor signal, attributed to the PTFE content, between electrodes before and after the electrochemical experiments. Although EDS provides localized surface information, measurements were conducted in triplicate on randomly selected regions to ensure more representative and reliable elemental data. For the electrode composed exclusively of Vulcan XC-72R, the fluor content after the electrochemical experiment decreased to 0.4 %, indicating an almost complete loss of PTFE surface. When 50 % of the biomass-waste derivates were incorporated to the GDL, the residual fluorine content was 3 %. In contrast, when the GDL was only prepared with biomass-waste derivates, the fluorine content remained as high as 35 %. These findings suggest that the inclusion of lignocellulosic material contributed to better PTFE retention on the electrodes surface, which may enhance the long-term stability and durability of the electrodes.

Moreover, Fig. 7c shows that in the case of unused PA 1000 °C, the distribution of Bi appears more heterogeneous compared to both Vulcan XC-72R and the 50–50 mixture. This heterogeneity in Bi dispersion may contribute to the lower overall formate production observed for this material, potentially by reducing the number of accessible sites for CO_2 activation or by promoting parasitic reactions, such as the HER, in Bi-deficient regions.

These compositional analysis results were consistent with those obtained from static contact angle (sCA) measurements. The absence of PTFE on the surface of the two electrodes used in the electroreduction experiments that contained Vulcan XC-72R was evident, as the water

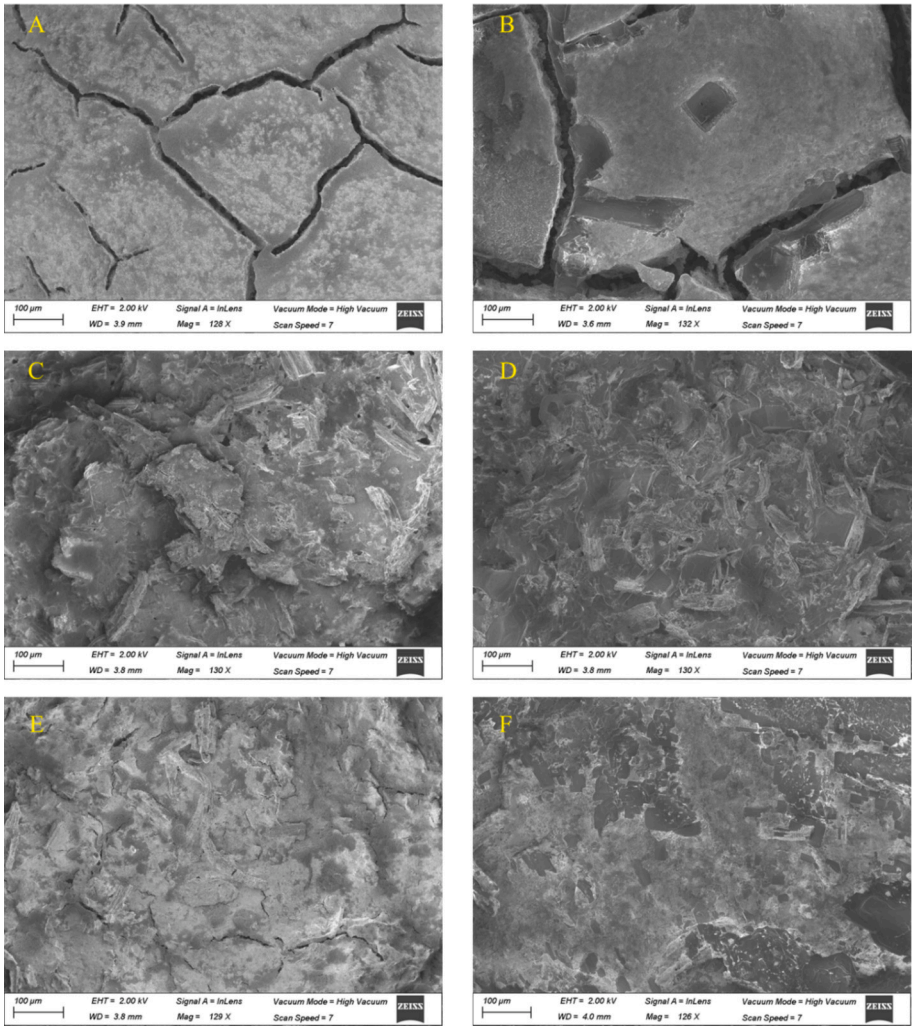

Fig. 6. SEM images of electrode surfaces: (A) unused Vulcan XC-72R, (B) used Vulcan XC-72R, (C) unused PA 1000 °C, (D) used PA 1000 °C, (E) unused PA 1000 °C-Vulcan XC-72R (50 %–50 %) and (F) used PA 1000 °C-Vulcan XC-72R (50 %–50 %). All electrodes were synthesized with vacuum and with the CL deposited.

droplet used for the measurement was completely absorbed, indicating a highly hydrophilic surface and confirming the loss of PTFE. In contrast, for the electrode totally synthesized from biomass-waste derivates, a measurable sCA of approximately 114° was obtained, indicating that the surface partially retained its hydrophobic properties (contact angle measurements included in Fig. S3 as Supplementary material). Contact angle measurements could not be performed on the fresh (unused) electrodes because their surfaces were excessively hydrophobic, preventing the water droplet from remaining on the surface.

4. Conclusions

This study highlights the potential of biomass-derived materials as sustainable alternatives to conventional carbon black in the fabrication of BioRem-GDEs for the electrochemical reduction of CO_2 to formate. Three lignocellulosic biomass sources—*Typha domingensis*, *Phragmites australis*, and *Cladium mariscus*—were successfully processed via hydrothermal carbonization, pyrolysis, and chemical activation to generate carbon materials suitable for use in the MPL of GDEs.

When blended with Vulcan XC-72R (50 wt%), these biomass-derived carbons produced GDEs capable of achieving formate concentrations of 1.8 $g{\cdot}L^{-1}$ at a current density of 90 $mA{\cdot}cm^{-2}$, with a Faradaic efficiency of approximately 80 % and an energy consumption of ~250 $kWh{\cdot}kmol^{-1}$. These performances are comparable or superior to those of electrodes made solely with commercial Vulcan [23], while offering environmental advantages such as reduced reliance on petroleum-based materials and the valorization of lignocellulosic biomass sources.

Overall, the results confirm the technical feasibility of BioRem-GDEs and support their potential role in sustainable CO_2 utilization strategies. Building on these findings, ongoing work is focused on assessing the long-term stability and performance of these electrodes in a more practical gas-phase electrochemical system [24], where only humidified CO_2 and GDEs are employed. This configuration—previously shown to produce high formate concentrations (>300 $g{\cdot}L^{-1}$) using Bi_2O_3 nanoparticles—has demonstrated significant improvements in both efficiency and productivity. However, further research is needed to optimize these systems and evaluate their scalability for industrial implementation.

CRediT authorship contribution statement

Guillermo Díaz-Sainz: Writing – review & editing, Writing – original draft, Supervision, Resources, Project administration, Methodology, Investigation, Funding acquisition, Formal analysis, Conceptualization. **Jose Antonio Abarca:** Writing – review & editing, Validation, Methodology, Investigation, Conceptualization. **Iker Uriarte-Porres:** Methodology, Investigation, Formal analysis, Conceptualization. **Álvaro Ramírez:** Writing – review & editing, Methodology, Investigation, Data curation, Conceptualization. **Martín Muñoz-Morales:** Writing – review & editing, Supervision, Methodology, Investigation, Formal analysis,

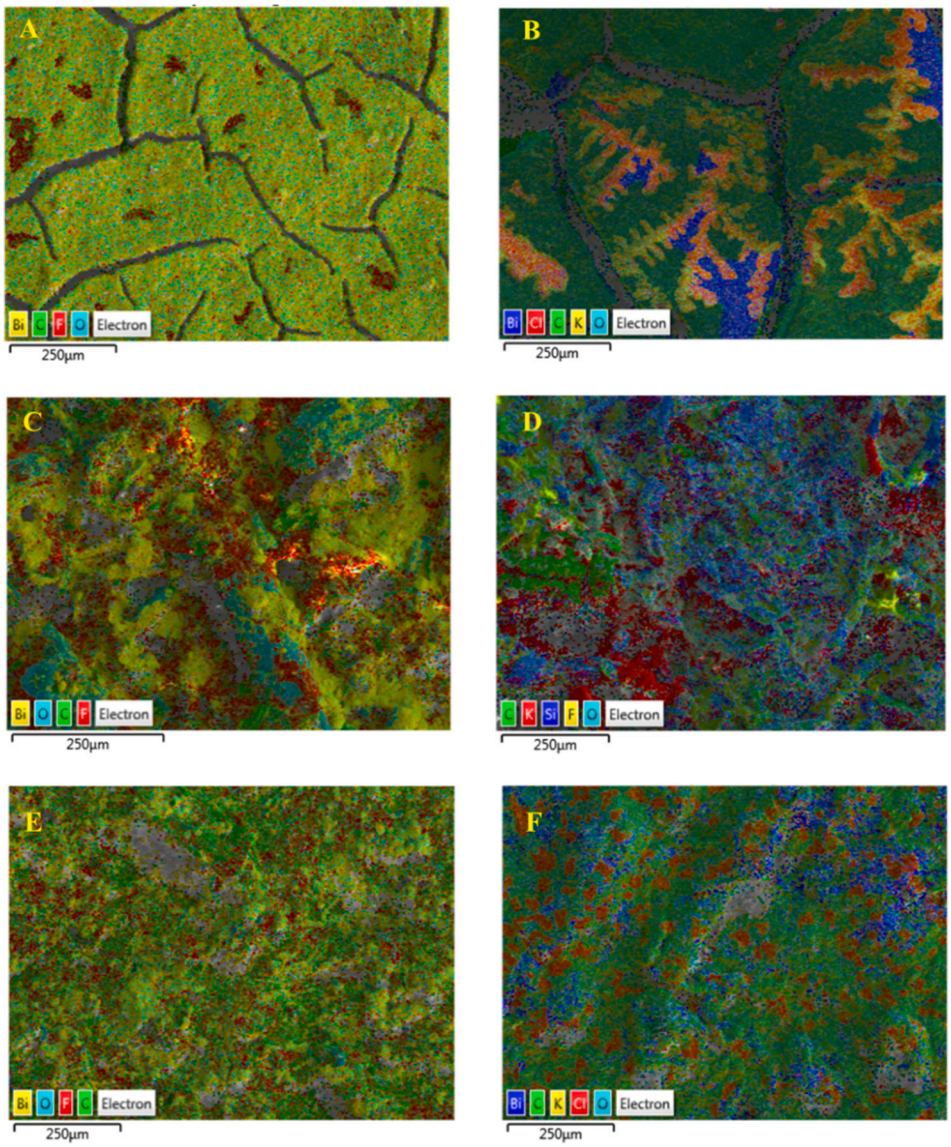

Fig. 7. EDS images of electrode surfaces: (A) unused Vulcan XC-72R, (B) used Vulcan XC-72R, (C) unused PA 1000 °C, (D) used PA 1000 °C, (E) unused PA 1000 °C-Vulcan XC-72R (50 %–50 %) and (F) used PA 1000 °C-Vulcan XC-72R (50 %–50 %). All electrodes were synthesized with vacuum and with the CL deposited.

Data curation, Conceptualization. **Ángel Irabien:** Writing – review & editing, Supervision, Resources, Project administration. **Javier Llanos:** Writing – review & editing, Supervision, Resources, Project administration, Methodology, Funding acquisition, Formal analysis, Data curation, Conceptualization. **Manuel Álvarez-Guerra:** Writing – review & editing, Writing – original draft, Supervision, Resources, Project administration, Methodology, Investigation, Funding acquisition, Conceptualization.

Declaration of competing interest

The authors declare that they have no known competing financial interests or personal relationships that could have appeared to influence the work reported in this paper.

Acknowledgements

The authors gratefully acknowledge financial support through projects TED2021-129810B-C21, PLEC2022-009398 (MCIN/AEI/10.13039/501100011033 and Unión Europea Next GenerationEU/PRTR), PID2022-138491OB-C31 and PID2022-141265OB-I00 (MICIU/AEI/10.13039/501100011033 and FEDER, UE) and the Complementary Plan in the area of "Energy and Renewable Hydrogen" (funded by Autonomous Community of Cantabria, Spain, and the European Union Next GenerationEU/PRTR). The present work is related to CAPTUS Project. This project has received funding from the European Union's Horizon 2020 - Research and Innovation Framework Programme under grant agreement No 101118265. Jose Antonio Abarca gratefully acknowledges the predoctoral research grant (FPI) PRE2021-097200.

Appendix A. Supplementary data

Supplementary data to this article can be found online at https://doi.org/10.1016/j.cej.2025.167825.

Data availability

No data was used for the research described in the article.

References

[1] NOAA Global Monitoring Laboratory, 2025. https://gml.noaa.gov/. (Accessed 8 August 2025).

[2] COP29 Azerbaijan - United Nations Climate Change Conference, 2025. https://cop29.az/en/home. (Accessed 8 August 2025).

[3] United Nations, 2025. https://www.un.org/. (Accessed 8 August 2025).

[4] J.F.D. Tapia, J.Y. Lee, R.E.H. Ooi, D.C.Y. Foo, R.R. Tan, A review of optimization and decision-making models for the planning of CO_2 capture, utilization and storage (CCUS) systems, Sustain. Prod. Consum. 13 (2018) 1–15, https://doi.org/10.1016/J.SPC.2017.10.001.

[5] M. Rumayor, J. Fernández-González, A. Domínguez-Ramos, A. Irabien, Deep decarbonization of the cement sector: a prospective environmental assessment of CO_2 recycling to methanol, ACS Sustain. Chem. Eng. 10 (2022) 267–278, https://doi.org/10.1021/acssuschemeng.1c06118.

[6] W. Zhang, Y. Hu, L. Ma, G. Zhu, Y. Wang, X. Xue, R. Chen, S. Yang, Z. Jin, Progress and perspective of electrocatalytic CO_2 reduction for renewable carbonaceous fuels and chemicals, Adv. Sci. 5 (2018) 1700275, https://doi.org/10.1002/ADVS.201700275.

[7] P.R. Yaashikaa, P. Senthil Kumar, S.J. Varjani, A. Saravanan, A review on photochemical, biochemical and electrochemical transformation of CO_2 into value-added products, J. CO_2 Util. 33 (2019) 131–147, https://doi.org/10.1016/j.jcou.2019.05.017.

[8] R.K. Bharatee, A.R. Quaff, S.K. Jaiswal, Advances in perovskite membranes for carbon capture & utilization: a sustainable approach to CO_2 emissions reduction – a review, J. Environ. Manag. 380 (2025) 124924, https://doi.org/10.1016/j.jenvman.2025.124924.

[9] G. Dativo, E. La Greca, L.F. Liotta, V. La Parola, M. Condorelli, G. Impellizzeri, G. Compagnini, S. Sciré, R. Fiorenza, Solar photothermo-catalytic conversion of CO_2 on phyllosilicates modified with Ni and CeO_2, J. CO_2 Util. 82 (2024) 102765, https://doi.org/10.1016/j.jcou.2024.102765.

[10] A. Ali, M. Qasim, S. Sakhi, G. Maduraiveeran, A.S. Alnaser, Electrochemical CO_2 reduction: advances, insights, challenges, and future directions, Mater. Today Sustain. 30 (2025) 101089, https://doi.org/10.1016/j.mtsust.2025.101089.

[11] G. Leonzio, A. Hankin, N. Shah, CO_2 electrochemical reduction: a state-of-the-art review with economic and environmental analyses, Chem. Eng. Res. Des. 208 (2024) 934–955, https://doi.org/10.1016/J.CHERD.2024.07.014.

[12] S.A. Al-Tamreh, M.H. Ibrahim, M.H. El-Naas, J. Vaes, D. Pant, A. Benamor, A. Amhamed, Electroreduction of carbon dioxide into formate: a comprehensive review, ChemElectroChem (2021) 1–15, https://doi.org/10.1002/celc.202100438.

[13] B. Li, L. Liu, M. Yue, Q. Niu, M. Li, T. Zhang, W. Xie, Q. Wang, Status and challenges for CO_2 electroreduction to CH_4: advanced catalysts and enhanced strategies, Green Chem. 26 (2024) 103–121, https://doi.org/10.1039/D3GC03893A.

[14] L. Kuo, C.T. Dinh, Toward efficient catalysts for electrochemical CO_2 conversion to C_2 products, Curr. Opin. Electrochem. 30 (2021) 100807, https://doi.org/10.1016/j.coelec.2021.100807.

[15] Business Analytiq - Formic Acid price index, 2025, in: https://businessanalytiq.com/procurementanalytics/index/formic-acid-price-index/. (Accessed 8 August 2025).

[16] L. An, R. Chen, Direct formate fuel cells: a review, J. Power Sources 320 (2016) 127–139, https://doi.org/10.1016/j.jpowsour.2016.04.082.

[17] Y. Wang, X. Xu, G. Dong, M. Zhang, K. Jiao, D.Y.C. Leung, Flexible fuel cells: a prospective review, Energy Rev. 3 (2024) 100099, https://doi.org/10.1016/j.enrev.2024.100099.

[18] X. Liu, Y. Wang, Z. Dai, D. Gao, X. Zhao, Electrochemical reduction of carbon dioxide to produce formic acid coupled with oxidative conversion of biomass, J. Energy Chem. 92 (2024) 705–729, https://doi.org/10.1016/j.jechem.2024.01.062.

[19] K. Fernández-Caso, G. Díaz-Sainz, M. Alvarez-Guerra, A. Irabien, Electroreduction of CO_2: advances in the continuous production of formic acid and formate, ACS Energy Lett. 8 (2023) 1992–2024, https://doi.org/10.1021/acsenergylett.3c00489.

[20] J.A. Abarca, M. Coz-Cruz, M. Alvarez-Guerra, G. Díaz-Sainz, A. Irabien, Experimental assessment of different reactor configuration approaches for direct CO_2 electroreduction to formic acid, Electrochim. Acta 525 (2025) 146182, https://doi.org/10.1016/j.electacta.2025.146182.

[21] J.A. Abarca, G. Díaz-Sainz, I. Merino-Garcia, G. Beobide, J. Albo, A. Irabien, Optimized manufacturing of gas diffusion electrodes for CO_2 electroreduction with automatic spray pyrolysis, J. Environ. Chem. Eng. 11 (2023) 109724, https://doi.org/10.1016/j.jece.2023.109724.

[22] G. Díaz-Sainz, K. Fernández-Caso, T. Lagarteira, S. Delgado, M. Alvarez-Guerra, A. Mendes, A. Irabien, Coupling continuous CO_2 electroreduction to formate with efficient Ni-based anodes, J. Environ. Chem. Eng. 11 (2023) 109171, https://doi.org/10.1016/j.jece.2022.109171.

[23] G. Díaz-Sainz, M. Alvarez-Guerra, J. Solla-Gullón, L. García-Cruz, V. Montiel, A. Irabien, CO_2 electroreduction to formate: continuous single-pass operation in a filter-press reactor at high current densities using Bi gas diffusion electrodes, J. CO_2 Util. 34 (2019) 12–19, https://doi.org/10.1016/j.jcou.2019.05.035.

[24] G. Díaz-Sainz, M. Alvarez-Guerra, B. Ávila-Bolívar, J. Solla-Gullón, V. Montiel, A. Irabien, Improving trade-offs in the figures of merit of gas-phase single-pass continuous CO_2 electrocatalytic reduction to formate, Chem. Eng. J. 405 (2021) 126965, https://doi.org/10.1016/j.cej.2020.126965.

[25] G. Díaz-Sainz, M. Alvarez-Guerra, A. Irabien, Continuous electroreduction of CO_2 towards formate in gas-phase operation at high current densities with an anion exchange membrane, J. CO_2 Util. 56 (2022) 101822, https://doi.org/10.1016/j.jcou.2021.101822.

[26] L.C. Weng, A.T. Bell, A.Z. Weber, Modeling gas-diffusion electrodes for CO_2 reduction, Phys. Chem. Chem. Phys. 20 (2018) 16973–16984, https://doi.org/10.1039/c8cp01319e.

[27] K. Yang, R. Kas, W.A. Smith, T. Burdyny, Role of the carbon-based gas diffusion layer on flooding in a gas diffusion electrode cell for electrochemical CO_2 reduction, ACS Energy Lett. 6 (2021) 33–40, https://doi.org/10.1021/acsenergylett.0c02184.

[28] Z. Xing, L. Hu, D.S. Ripatti, X. Hu, X. Feng, Enhancing carbon dioxide gas-diffusion electrolysis by creating a hydrophobic catalyst microenvironment, Nat. Commun. 12 (2021) 136, https://doi.org/10.1038/s41467-020-20397-5.

[29] Y. Wu, L. Charlesworth, I. Maglaya, M.N. Idros, M. Li, T. Burdyny, G. Wang, T. E. Rufford, Mitigating electrolyte flooding for electrochemical CO_2 reduction via infiltration of hydrophobic particles in a gas diffusion layer, ACS Energy Lett. 7 (2022) 2884–2892, https://doi.org/10.1021/acsenergylett.2c01555.

[30] J.A. Abarca, G. Díaz-Sainz, I. Merino-Garcia, A. Irabien, J. Albo, Photoelectrochemical CO_2 electrolyzers: From photoelectrode fabrication to reactor configuration, J. Energy Chem. 85 (2023) 455–480, https://doi.org/10.1016/j.jechem.2023.06.032.

[31] A. Gawel, T. Jaster, D. Siegmund, J. Holzmann, H. Lohmann, E. Klemm, U.-P. Apfel, Electrochemical CO_2 reduction-the macroscopic world of electrode design, reactor concepts & economic aspects, ISciencie 25 (2022) 104011, https://doi.org/10.1016/j.isci.

[32] C.P. O'Brien, R.K. Miao, A. Shayesteh Zeraati, G. Lee, E.H. Sargent, D. Sinton, CO_2 electrolyzers, Chem. Rev. 124 (2024) 3648–3693, https://doi.org/10.1021/acs.chemrev.3c00206.

[33] D. Wakerley, S. Lamaison, J. Wicks, A. Clemens, J. Feaster, D. Corral, S.A. Jaffer, A. Sarkar, M. Fontecave, E.B. Duoss, S. Baker, E.H. Sargent, T.F. Jaramillo, C. Hahn, Gas diffusion electrodes, reactor designs and key metrics of low-temperature CO_2 electrolysers, Nat. Energy 7 (2022) 130–143, https://doi.org/10.1038/s41560-021-00973-9.

[34] J.A. Abarca, G. Díaz-Sainz, A. Irabien, Inhibiting salt precipitation on the gas diffusion electrode surface in gas-phase CO_2 electroreduction to formate by using an acidic anolyte, J. CO_2 Util. 86 (2024) 102897, https://doi.org/10.1016/j.jcou.2024.102897.

[35] L.P. Chi, Z.Z. Niu, X.L. Zhang, P.P. Yang, J. Liao, F.Y. Gao, Z.Z. Wu, K. Bin Tang, M. R. Gao, Stabilizing indium sulfide for CO_2 electroreduction to formate at high rate by zinc incorporation, Nat. Commun. 12 (2021) 5835, https://doi.org/10.1038/s41467-021-26124-y.

[36] Z. Bitar, A. Fecant, E. Trela-Baudot, S. Chardon-Noblat, D. Pasquier, Electrocatalytic reduction of carbon dioxide on indium coated gas diffusion electrodes—comparison with indium foil, Appl. Catal. B Environ. 189 (2016) 172–180, https://doi.org/10.1016/J.APCATB.2016.02.041.

[37] M. Alvarez-Guerra, S. Quintanilla, A. Irabien, Conversion of carbon dioxide into formate using a continuous electrochemical reduction process in a lead cathode, Chem. Eng. J. 207-208 (2012) 278–284, https://doi.org/10.1016/j.cej.2012.06.099.

[38] M. Alvarez-Guerra, A. Del Castillo, A. Irabien, Continuous electrochemical reduction of carbon dioxide into formate using a tin cathode: comparison with lead cathode, Chem. Eng. Res. Des. 92 (2014) 692–701, https://doi.org/10.1016/j.cherd.2013.11.002.

[39] Y.J. Ko, J.Y. Kim, W.H. Lee, M.G. Kim, T.Y. Seong, J. Park, Y.J. Jeong, B.K. Min, W. S. Lee, D.K. Lee, H.S. Oh, Exploring dopant effects in stannic oxide nanoparticles for CO_2 electro-reduction to formate, Nat. Commun. 13 (2022) 2205, https://doi.org/10.1038/s41467-022-29783-7.

[40] A. Del Castillo, M. Alvarez-Guerra, J. Solla-Gulló N, A. Sá Ez, V. Montiel, A. Irabien, Sn nanoparticles on gas diffusion electrodes: synthesis, characterization and use for continuous CO_2 electroreduction to formate, J. CO_2 Util. 18 (2017) 222–228, https://doi.org/10.1016/j.jcou.2017.01.021.

[41] S. Ma, K. Wu, S. Fan, Y. Li, Q. Xie, J. Ma, L. Yang, Electrocatalytic CO_2 reduction enhanced by Sb doping in MOF-derived carbon-supported Bi-based materials, Sep. Purif. Technol. 339 (2024) 126520, https://doi.org/10.1016/j.seppur.2024.126520.

[42] G. Díaz-Sainz, M. Alvarez-Guerra, J. Solla-Gullón, L. García-Cruz, V. Montiel, A. Irabien, Gas–liquid–solid reaction system for CO_2 electroreduction to formate without using supporting electrolyte, AICHE J. 66 (2020) e16299, https://doi.org/10.1002/aic.16299.

[43] Y. Wu, S. Garg, M. Li, M.N. Idros, Z. Li, R. Lin, J. Chen, G. Wang, T.E. Rufford, Effects of microporous layer on electrolyte flooding in gas diffusion electrodes and selectivity of CO_2 electrolysis to CO, J. Power Sources 522 (2022) 230998, https://doi.org/10.1016/J.JPOWSOUR.2022.230998.

[44] E. Llobet, Gas sensors using carbon nanomaterials: a review, Sensors Actuators B Chem. 179 (2013) 32–45, https://doi.org/10.1016/j.snb.2012.11.014.

[45] H. Siddiqui, U. Ali, I.A. Sahito, S.A. Malik, K.C. Sun, N. Mengal, Comprehensive review of carbon materials as counter electrodes in dye-sensitized solar cells: efficiency assessment and deposition methods, Mater. Sci. Semicond. Process. 172 (2024) 108074, https://doi.org/10.1016/j.mssp.2023.108074.

[46] Y. Holade, N.E. Sahin, K. Servat, T.W. Napporn, K.B. Kokoh, Recent advances in carbon supported metal nanoparticles preparation for oxygen reduction reaction in low temperature fuel cells, Catalysts 5 (2015) 310–348, https://doi.org/10.3390/catal5010310.

[47] United States Enviromental Protection Agency, Chapter 6: Organic Chemical Process Industry, Fifth edition, 1983, p. 1.

[48] A.P.R.A. Ferreira, R.C.P. Oliveira, M.M. Mateus, D.M.F. Santos, A review of the use of electrolytic cells for energy and environmental applications, Energies 16 (2023) 1593, https://doi.org/10.3390/en16041593.
[49] S. Ashraf, Q. Ali, Z.A. Zahir, S. Ashraf, H.N. Asghar, Phytoremediation: environmentally sustainable way for reclamation of heavy metal polluted soils, Ecotoxicol. Environ. Saf. 174 (2019) 714–727, https://doi.org/10.1016/J.ECOENV.2019.02.068.
[50] A. Mahar, P. Wang, A. Ali, M.K. Awasthi, A.H. Lahori, Q. Wang, R. Li, Z. Zhang, Challenges and opportunities in the phytoremediation of heavy metals contaminated soils: a review, Ecotoxicol. Environ. Saf. 126 (2016) 111–121, https://doi.org/10.1016/J.ECOENV.2015.12.023.
[51] M.H. Saleem, S. Ali, M. Rehman, M.S. Rana, M. Rizwan, M. Kamran, M. Imran, M. Riaz, M.H. Soliman, A. Elkelish, L. Liu, Influence of phosphorus on copper phytoextraction via modulating cellular organelles in two jute (*Corchorus capsularis* L.) varieties grown in a copper mining soil of Hubei Province, China, Chemosphere 248 (2020) 126032, https://doi.org/10.1016/J.CHEMOSPHERE.2020.126032.
[52] M.A. Maine, H.R. Hadad, N.E. Camaño Silvestrini, E. Nocetti, G.C. Sanchez, M. A. Campagnoli, Cr, Ni, and Zn removal from landfill leachate using vertical flow wetlands planted with Typha domingensis and Canna indica, Int. J. Phytoremediation 24 (2022) 66–75, https://doi.org/10.1080/15226514.2021.1926909.
[53] M. Prica, G. Andrejić, J. Šinžar-Sekulić, T. Rakić, Ž. Dželetović, Bioaccumulation of heavy metals in common reed (Phragmites australis) growing spontaneously on highly contaminated mine tailing ponds in Serbia and potential use of this species in phytoremediation, Bot. Serbica 43 (2019) 85–95, https://doi.org/10.2298/BOTSERB1901085P.
[54] M. Trojanowska, Reclamation of polluted land in urban renewal projects. Literature review of suitable plants for phytoremediation, Environ. Challenges 13 (2023) 100749, https://doi.org/10.1016/j.envc.2023.100749.
[55] M.V.T. Gomes, R.R. de Souza, V.S. Teles, É. Araújo Mendes, Phytoremediation of water contaminated with mercury using Typha domingensis in constructed wetland, Chemosphere 103 (2014) 228–233, https://doi.org/10.1016/j.chemosphere.2013.11.071.
[56] S. Rezania, J. Park, P.F. Rupani, N. Darajeh, X. Xu, R. Shahrokhishahraki, Phytoremediation potential and control of Phragmites australis as a green phytomass: an overview, Environ. Sci. Pollut. Res. 26 (2019) 7428–7441, https://doi.org/10.1007/s11356-019-04300-4.
[57] P. Bartczak, M. Wawrzkiewicz, S. Borysiak, T. Jesionowski, *Cladium mariscus* saw-sedge versus sawdust—efficient biosorbents for removal of hazardous textile dye C. I. basic blue 3 from aqueous solutions, Processes 10 (2022) 586, https://doi.org/10.3390/pr10030586.
[58] P. Bartczak, S. Żółtowska, M. Norman, Ł. Klapiszewski, J. Zdarta, A. Komosa, I. Kitowski, F. Ciesielczyk, T. Jesionowski, Saw-sedge Cladium mariscus as a functional low-cost adsorbent for effective removal of 2,4-dichlorophenoxyacetic acid from aqueous systems, Adsorption 22 (2016) 517–529, https://doi.org/10.1007/s10450-015-9708-2.
[59] Á. Ramírez, M. Muñoz-Morales, F.J. Fernández-Morales, J. Llanos, Innovative carbon materials from lignocellulosic wastes for electrochemical hydrogen peroxide production: bridging biomass conversion and material properties, J. Environ. Chem. Eng. 12 (2024) 112985, https://doi.org/10.1016/j.jece.2024.112985.
[60] J. Winkler, M. Ježová, R. Punčochář, E. Hurajová, P.M. Barroso, T. Kopta, D. Semerádová, M.D. Vaverková, Fire hazard: undesirable ecosystem function of orchard vegetation, Fire 6 (2023) 25, https://doi.org/10.3390/FIRE6010025.
[61] K. Fernández-Caso, A. Peña-Rodríguez, J. Solla-Gullón, V. Montiel, G. Díaz-Sainz, M. Alvarez-Guerra, A. Irabien, Continuous carbon dioxide electroreduction to formate coupled with the single-pass glycerol oxidation to high value-added products, J. CO_2 Util. 70 (2023) 102431, https://doi.org/10.1016/j.jcou.2023.102431.
[62] I. Merino-Garcia, L. Tinat, J. Albo, M. Alvarez-Guerra, A. Irabien, O. Durupthy, V. Vivier, C.M. Sánchez-Sánchez, Continuous electroconversion of CO_2 into formate using 2 nm tin oxide nanoparticles, Appl. Catal. B Environ. 297 (2021) 120447, https://doi.org/10.1016/j.apcatb.2021.120447.
[63] J.A. Abarca, L. Warmuth, A. Rieder, A. Dutta, S. Vesztergom, P. Broekmann, A. Irabien, G. Díaz-Sainz, GDE stability in CO_2 electroreduction to formate: the role of ionomer type and loading, ACS Catal. 15 (2025) 8753–8767, https://doi.org/10.1021/acscatal.5c02052.
[64] Y. Kong, M. Liu, H. Hu, Y. Hou, S. Vesztergom, M. de J. Gálvez-Vázquez, I. Zelocualtecatl Montiel, V. Kolivoška, P. Broekmann, Cracks as efficient tools to mitigate flooding in gas diffusion electrodes used for the electrochemical reduction of carbon dioxide, Small Methods 6 (2022) 2200369, https://doi.org/10.1002/smtd.202200369.
[65] X. Cao, B. Wulan, B. Zhang, D. Tan, J. Zhang, Defect evolution of hierarchical SnO_2 aggregates for boosting CO_2 electrocatalytic reduction, J. Mater. Chem. A 9 (2021) 14741–14751, https://doi.org/10.1039/D1TA03530D.
[66] M. Muñoz-Morales, A. Ramírez, A. Cañizares, J. Llanos, C. Ania, Evaluating key properties of carbon materials as cathodes for the electrogeneration of hydrogen peroxide, Carbon 210 (2023) 118082, https://doi.org/10.1016/j.carbon.2023.118082.
[67] S. Pérez-Rodríguez, E. Pastor, M.J. Lázaro, Electrochemical behavior of the carbon black Vulcan XC-72R: influence of the surface chemistry, Int. J. Hydrog. Energy 43 (2018) 7911–7922, https://doi.org/10.1016/j.ijhydene.2018.03.040.